Featured in Physics

Dynamic Allometry of Nuclei in Early Embryos of *Caenorhabditis elegans*

Rolf Fickentscher,[1] Tomoko Ozawa,[2] Akatsuki Kimura,[2,3] and Matthias Weiss[1,*]

[1]*Experimental Physics I, University of Bayreuth, Universitätsstraße 30, D-95447 Bayreuth, Germany*
[2]*Cell Architecture Laboratory, National Institute of Genetics, Yata 1111, Mishima, Shizuoka 411-8540, Japan*
[3]*Department of Genetics, The Graduate University for Advanced Studies (SOKENDAI), Yata 1111, Mishima, Shizuoka 411-8540, Japan*

(Received 15 December 2022; revised 14 November 2023; accepted 18 December 2023; published 13 February 2024)

Allometric relations between two observables are a widespread phenomenon in biology. The volume of nuclei, for example, has frequently been reported to scale linearly with cell volume, $V_N \sim V_C$, but conflicting, sublinear power-law correlations have also been found. Given that nuclei are vital organelles that harbor and maintain the DNA of cells, an understanding of allometric nuclear volumes that ultimately define the concentration and accessibility of chromatin is of great interest. Using the model organism *Caenorhabditis elegans*, we show here that the allometry of nuclei is a dynamically adapting phenomenon; i.e., we find $V_N \sim V_C^{\alpha}$ with a time-dependent scaling exponent α ("dynamic allometry"). This finding is due to relaxation growth of nuclear volumes at a rate that scales with cell size. If cell division stops the relaxation of nuclei in a premature stage, $\alpha < 1$ is observed, whereas completion of relaxation yields $\alpha = 1$ ("isometry"). Our experimental data are well captured by a simple and supposedly generic model in which nuclear size is determined by the available membrane area that can be integrated into the nuclear envelope to relax the expansion pressure from decondensed chromatin. Extrapolation of our results to growing and proliferating cells suggests that isometric scaling of cell and nuclear volumes is the generic case.

DOI: 10.1103/PhysRevX.14.011016 Subject Areas: Biological Physics

I. INTRODUCTION

Allometric relations between two observables X and Y are an intriguing and common phenomenon in biology. Prominent examples for an allometric scaling, $Y = bX^{\alpha}$, include the metabolic rate and lifespan of animals, which scale sublinearly with body mass (with $\alpha \approx 3/4$ and $\alpha \approx 0.15$, respectively) [1]; the rate of neurodegeneration, which scales with the maximum lifespan of an animal (with α depending on the gene involved) [2]; or an isometric ($\alpha = 1$) relation between the volumes of cells and nucleoli in larvae [3]. It is also known that the volume of the cell nucleus correlates with the amount of enclosed DNA [4–7], and it also scales approximately linearly with cell size [4,8–17]. In fact, although a constant amount of DNA can feature a wide range of cell and nucleus sizes, the ratio of nucleus and cell volume, $\phi = V_N/V_C \approx 0.1$, appears to be surprisingly constant, e.g., in fission yeast [13], in mouse macrophages [18], and in (human) HeLa cells [19], whereas elevated values for ϕ have often been reported for cancer cells [20–22]. Notably, the nucleus volume eventually determines the concentration, accessibility, and mobility of chromatin [23], thereby affecting the regulatory and transcriptional activities of the cell. Alterations in these activities are often associated with severe diseases, such as cancer.

At first glance, an isometric relation $V_N \sim V_C$ can be rationalized straightforwardly and without knowledge of molecular details by assuming that the amount of building material for nuclei is fixed by the cell volume [24]; i.e., nuclei can only be made from these limited resources. Yet, nuclei in early embryos and larvae of the model organism *Caenorhabditis elegans* have been reported not to follow an isometric scaling with cell size [3,14]. These findings suggest that an isometric scaling of nuclei with cell volume is not only determined by an elaborate but passive partitioning of limiting cell material but may rather invoke active mechanisms for sensing and adapting cell and/or nuclear volumes.

A potential pitfall of allometric relations is, in general, the tacit assumption that the related observables are at a steady state. Kinetic or dynamic changes beyond steady-state fluctuations are not taken into account. For example, cells and/or nuclei may change their volumes over time, potentially compromising the interpretation of apparent allometries and ϕ values. This caveat also touches on the

*matthias.weiss@uni-bayreuth.de

simple rationale for an isometric relation $V_N \sim V_C$ in the previous paragraph: The synthesis of new proteins and lipids, a typical and vital process of virtually every cell, may provide additional material for the growth of the nucleus over time; i.e., the idea of partitioning a constant amount of limited resources may be too simplistic. In general, one can expect a "dynamic allometry," where the scaling exponent α explicitly depends on the time elapsed since the last cell division.

So far, several potential determinants for achieving a constant ratio ϕ between cell and nuclear volume have been proposed, e.g., the perinuclear endoplasmic reticulum and its transport by dynein in *Xenopus* and sea urchin [25,26], or histone chaperones and their transport in *Xenopus* [25,27]. In addition, the difference in nuclear size between two related *Xenopus* species was explained by a different activity of nuclear import [15], and a post-translational modification of so-called importins was shown to act as a sensor of the volume-to-area ratio of cells [28]. A genetic screen in fission yeast revealed that several genes are involved in nuclear size regulation, including the nuclear import machinery [29]. However, no consensus has yet been reached on the core mechanisms that drive (dynamic) nuclear size adaptation across species and organisms to maintain an allometric relationship with cell size.

Given the limited knowledge of the driving forces and dynamic maintenance aspects underlying a potentially generic allometric relation between cell and nuclear volume, we hypothesized that robust physical cues are key to dynamically adjusting nuclear volume toward an isometric relation, $V_N \sim V_C$, with a constant ratio ϕ. To test this hypothesis experimentally, we aimed to use a native tissue of a living organism, rather than relying on immortalized culture cells grown on artificial substrates. In addition, we aimed to reduce complexity as much as possible by avoiding a net growth of the tissue. The embryos of the developmental model organism *Caenorhabditis elegans* readily meet these requirements, as well as being highly amenable to light microscopy-based quantification: *C. elegans* embryogenesis proceeds autonomously within a protective chitin egg shell, with an invariant cell lineage tree and highly reproducible cell divisions at a conserved total volume; i.e., cells are successively smaller blastomeres (see also Ref. [30] for an introduction). Furthermore, the early development of individual embryos follows a stereotypical protocol that appears to be governed by physical cues: Cell positions and migration paths before gastrulation can be captured very well with a simple model that relies on the mutual repulsion of cells within the engulfing eggshell, with anticorrelated cell volumes and division times [31–33].

Because of their convenient properties, *C. elegans* embryos have been used to study cell-size-dependent scaling of mitotic spindles, centrosomes, cytokinetic contractile rings, and nucleoli [14,23,34–38]. However, nuclear volumes have only been partially assessed in *C. elegans* embryos, and they appear to deviate from a simple linear scaling with cell volume [3,14]. Going beyond these earlier approaches, we have quantified cell and nucleus volumes in *C. elegans* embryos over time and used these data to test our aforementioned hypothesis. We find that nuclei exhibit a relaxation-like growth toward an asymptotic size that scales isometrically with cell size. Because of the competition of two timescales (relaxation of nuclei versus cell cycle time), the scaling exponent α in the relation $V_N \sim V_C^{\alpha}$ explicitly depends on the time at which nuclear volumes are quantified ("dynamic allometry"). Emphasizing the dynamic aspect further, the nuclear relaxation rate scales inversely with cell volume. All experimentally found scalings are well captured by a simple and generic model, suggesting a robust mechanism for dynamically achieving and maintaining an isometric relation between cell and nuclear volumes even beyond the organism studied here.

II. MATERIALS AND METHODS

To quantify nuclear sizes from confocal image stacks, we used the CAL1531 strain (GFP::PH(PLC1δ1), mCherry :: his-58, GFP :: LEM-2) in which the plasma membrane and the nuclear envelope are highlighted by a green fluorescent protein construct. The CAL1531 strain was constructed by crossing OD58 [39] and OD83 [40] strains. All strains were maintained with standard procedures [41]. Hydroxyurea was used to prolong the time from pronuclear meeting to nuclear envelope breakdown [42,43]. In this study, gravid worms were soaked in 10 mg/ml hydroxyurea in M9 buffer for one hour.

For imaging, adult hermaphrodites were dissected in 0.75× egg-salt buffer (118 mM NaCl, 40 mM KCl, 3.4 mM $CaCl_2$, 3.4 mM $MgCl_2$, 5 mM HEPES pH 7.2). Isolated embryos were transferred to 18×18 mm^2 coverslips coated with poly-L-lysine, mounted on a glass slide, and sealed with VALAP. Confocal imaging of these specimens was performed at 25 °C using a CSU-X1 spinning-disk confocal system (Yokogawa, Tokyo, Japan) mounted on a BX71 microscope (Olympus, Tokyo, Japan) equipped with an UPlanSApo 100x/1.40 objective (Olympus) and an EM-CCD camera (iXon, Andor Technology, Belfast, Northern Ireland). The setup was controlled by the MetaMorph imaging software (Molecular Devices, Sunnyvale, CA, USA). Z-stacks of 16 imaging planes (2 μm separation) were acquired every 2 min for embryos in the two- to eight-cell stage, and every 75 s for the 24-cell stage. Each imaging plane was illuminated with a 488-nm laser for 20 ms. An example of a confocal image at the four-cell state is shown in Fig. 1(a). The image stacks were then analyzed using Imaris (Bitplane, Zurich, Switzerland). The borders of nuclei and cells were manually traced for each Z section, and the resulting volumes were calculated by the software. An example of the segmented image stack is shown in Fig. 1(b) [same embryo as in Fig. 1(a)].

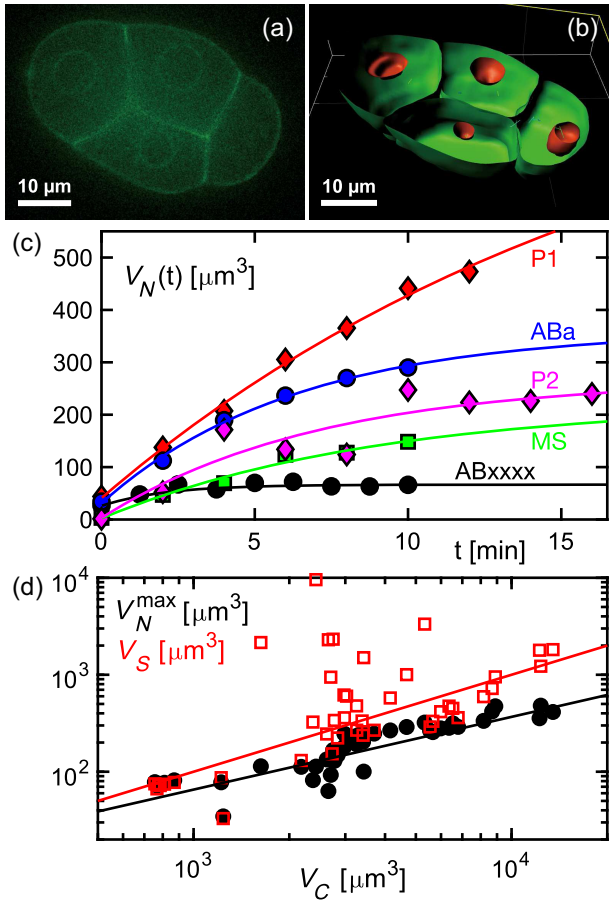

FIG. 1. (a) Representative confocal image of a *C. elegans* embryo in the four-cell state with the green fluorescence highlighting plasma membrane and nuclear envelope (over a residual fluorescence background in the cytoplasm and nucleoplasm). (b) After manual segmentation of the entire image stack, the identified cell boundaries (green) and nuclear envelopes (red) allow for quantifying the respective volumes. (c) Representative data for the growth kinetics of the nuclear volume V_N for single cells of the somatic (ABa, ABxxxx, MS) and germline (P1, P2) lineages in a single embryo. The experimental data (symbols) can be well fitted by Eq. (1) (solid lines, $0.81 < R^2 < 0.99$). (d) Largest nuclear volume $V_N^{\max}$ observed experimentally before cell division (black circles, $n = 5$ embryos), are linked to the cell volume V_C by a sublinear relation $V_N^{\max} \approx 0.37 V_C^{0.75}$ (black line, $R^2 = 0.76$). In contrast, the asymptotic steady-state volume $V_S = V_0 + V_1$ (red open squares) obtained by Eq. (1) roughly follows an isometric relation $V_S = V_C/10$ (red line), albeit with considerable fluctuations (hence only $R^2 = 0.33$).

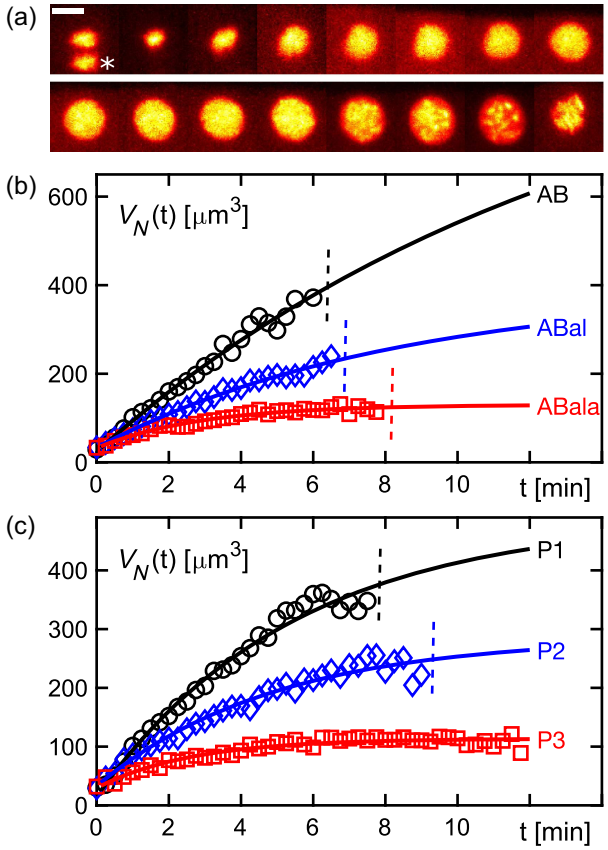

FIG. 2. (a) Representative image sequence of fluorescently labeled chromatin in the P2 cell (1 min between consecutive frames, scale bar: 5 µm). In the first image (anaphase of the mother cell, P1), the chromatin of the second daughter cell (EMS) is marked with an asterisk. The area of the chromatin signal is approximately circular; i.e., nuclei were approximately spherical. (b),(c) Representative time course of nuclear volumes, $V_N(t)$, for differently sized cells of the somatic (AB, ABal, ABala) and germline (P1, P2, P3) lineages. Symbols represent the mean of $n = 9$ untreated embryos. The standard error of the mean, reflecting embryo-to-embryo variation, was less than or equal to the symbol size for virtually all data points. Fits according to Eq. (1) are shown as solid lines ($0.92 < R^2 < 0.99$). For large cells, the nuclear expansion was stopped by the next division event (dashed vertical lines), whereas nuclei of smaller cells had sufficient time to reach their final volume.

The findings from confocal imaging were complemented with previously reported light-sheet microscopy data on strain OD95 (GFP: : PH(PLC1δ1), mCherry :: his-58) [44] in which the plasma membrane and chromatin were fluorescently labeled with different colors. In brief, three-dimensional stacks of 51 individual dual-color images were acquired every 30 s at 22.5 °C using a custom-built light-sheet microscope [45] with a spatial resolution (full-width half maximum) of 495 nm (in-plane) and 1.2 µm (sheet thickness). Time series covered the development from the single-cell state to the onset of gastrulation. A faithful extraction of cell volumes for all cells along the lineage tree until gastrulation has been performed and reported already (see Refs. [32,33,46] for details). Temperature-dependent data (previously published in Ref. [33]) are based on strain XA3501 (GFP::H2B, GFP::tbb-2) [47], featuring labeled histones and tubulin.

For the current study, we have used the median volume obtained from the time courses of individual embryos, averaged over all embryos, as the final volume of each cell, V_C. In addition to untreated embryos ($n = 9$), images of

embryos with the chitin eggshell removed ($n = 9$) were also included [46] to investigate the influence of the rigid confining ellipsoidal boundary conditions. Moreover, we also included embryos that were forced via RNAi treatment to be larger (target: C27D9.1; $n = 7$) or smaller (target: *ima-3*; $n = 3$) than normal embryos [32] to probe effects of the overall embryonic length scale.

To determine the approximate volumes of nuclei, V_N, we reexamined these extensive sets of light-sheet images. Chromatin fluorescence was seen in a roughly circular shape in all embryos, cells, and images (except for deformations during cell division); see Fig. 2(a) for an example. This finding indicates an almost spherical chromatin assembly as the orientation of the embryos with respect to the imaging plane was random. Therefore, at each time point, we determined the maximum chromatin area A for each cell across the image stack by automatic thresholding (using the local minimum of the bimodal pixel intensity distribution in maximum-intensity projections) and determined from this the approximate nucleus volume as $V_N = 4A^{3/2}/(3\sqrt{\pi})$. For temporal registration, we have assigned the starting point $t = 0$ for each newborn cell to the image stack acquired 90 s after the onset of anaphase in the respective mother cell. At this time, the daughter nuclei were almost spherical again [cf. Fig. 2(a)]. Varying this choice in the range of 120–180 s after anaphase onset changed the values of the relaxation time τ but did not affect the scaling discussed in the main text.

III. RESULTS AND DISCUSSION

A. Experiments reveal a dynamic allometry of nuclei

As a first step to assess and monitor nuclear volumes in *C. elegans* embryos over time, we used three-dimensional reconstructions from time-resolved confocal imaging (see Sec. II). Since confocal microscopy allows for diffraction-limited imaging at very high spatial resolution in all dimensions (due to the use of an objective with a high numerical aperture), we reasoned that cellular structures would be best resolved with this approach. Stacks of confocal images [see Fig. 1(a) for a representative image in the four-cell state] allowed us to obtain complete three-dimensional reconstructions of the embryo [see Fig. 1(b) for an example] from which the cell and nucleus volumes were determined by image segmentation. To mitigate the effects of bleaching-induced poisoning of the embryo and because of the time-consuming image acquisition, only a few data points $V_N(t)$ per cell could be obtained with this high-resolution imaging approach. As a result, we found that even the data for single embryos, i.e., without any averaging, clearly show an increase of the nucleus volume over time in all tested cells [see Fig. 1(c) for examples]. In addition to a general increase in nuclear volume over time, we observed a convergence to plateau values for small cells, e.g., for P2. In contrast, larger cells (e.g., P1) did not reach a plateau, but nuclear growth was ended by the onset of cell division.

Since cell division times and cell volume are anticorrelated in the early embryo [32], we reasoned that larger cells would eventually also converge to a plateau if given sufficient time before initiating the next cell division. However, prolonging cell cycle times by genetic or pharmaceutical means is intricate and prone to inducing unwanted (additional) effects. With this caveat in mind, we used a well-characterized approach [42,43] and treated embryos with hydroxyurea to delay the first embryonic cell division. Consistent with our caveat, we note that a cumulation of defects due to hydroxyurea treatment prevents cell division of P1 already in the two-cell state [42]. In accordance with earlier observations [42,43], we observed that hydroxyurea treatment delayed cell division and increased the observable nuclear expansion period substantially (see Fig. S1 in the Supplemental Material [48]). At the same time, the apparently unlimited growth of nuclear volumes in untreated embryos was seen to saturate in treated embryos, supporting the above reasoning. From this finding (and additional data in Fig. 3, discussed below), we conclude that all nuclei indeed undergo relaxation growth toward a plateau value, but the process is stopped in a premature stage by the early onset of mitosis in large cells. Consequently, an allometric relation will depend on the time at which the nuclear volume is quantified (unless stationarity can be assumed).

To evaluate the time course of all nuclear volumes, we fitted a simple relaxation law

$$V_N(t) = V_0 + V_1(1 - e^{-t/\tau}) \tag{1}$$

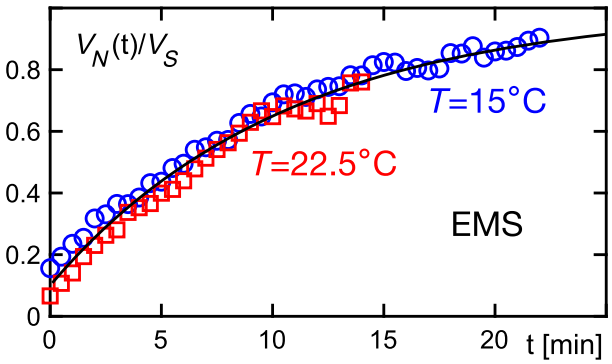

FIG. 3. When the ambient temperature is lowered from 22.5 °C to 15 °C, the cell cycle time is prolonged [33], providing additional time for the nuclei to relax to their asymptotic volume. The example curves refer to EMS cells at the indicated temperatures. For better comparison of the relaxation, the fluctuating asymptotic volume V_S is divided out since no consistent trend of the fit parameters in Eq. (1) as a function of temperature was observed (Fig. S2 in the Supplemental Material [48]). A single relaxation curve according to Eq. (1) (black line) is also shown for comparison.

to our experimental data [see Fig. 1(c) for representative examples] and extracted the asymptotic volume $V_S = V_0 + V_1$. In addition, we determined for each cell the maximum nuclear volume $V_N^{\max}$ observed before cell division. In line with previous observations [14], the maximum nuclear volume was found to scale sublinearly with cell volume on average, $V_N^{\max} \sim V_C^{0.75}$ [Fig. 1(d)]. In contrast, the extrapolated asymptotic volume V_S follows, on average, an isometric relation $V_S = \phi V_C$ with $\phi \approx 0.1$ [Fig. 1(d)]. The discrepancy between the scaling of $V_N^{\max}$ and V_S emphasizes the notion of a time-dependent allometry.

Because of the limited number of data points for each cell and since the plateau values for nuclear volumes are often not reached, the fit parameters in Eq. (1) are plagued by considerable statistical uncertainties, which explains the strong jitter in V_S as compared to $V_N^{\max}$ [Fig. 1(d)]. To reduce the jitter by increasing the number of data points per cell, we aimed to complement the data from confocal microscopy with an imaging technique that allows for a higher temporal resolution, even if we had to compromise on spatial resolution.

As a complementary technique, we have chosen light-sheet microscopy (see Sec. II), which allows for faster imaging with negligible phototoxicity, albeit with the drawback of a lower spatial resolution. Light-sheet microscopy also overcomes a pertinent problem in confocal microscopy, namely, that imaging of unconstrained embryos beyond the four-cell state can partially miss cells that are distal from the objective. Here, three-dimensional stacks of 51 individual dual-color images were acquired every 30 s with negligible bleaching, allowing for a considerably better sampling of volumes over time. Chromatin images revealed that nuclei were almost circular in shape in all image planes, indicating a nearly spherical shape of nuclei during interphase [Fig. 2(a)]. We therefore approximated the nuclear volume as $V_N = 4A^{3/2}/(3\sqrt{\pi})$ via the largest nucleus area A in the image stack (see Sec. II). Notably, these chromatin-based volume estimates were, on average, 10%–15% lower than those obtained by confocal imaging and reconstruction of the surrounding nuclear envelope.

Using the light-sheet imaging data, with an improved number of data points, we observed that nuclear volumes indeed followed an expansion that is well described by Eq. (1); see examples in Figs. 2(b) and 2(c). Notably, this finding was not altered when evaluating embryos that were left untreated, genetically modified to be larger or smaller (see Sec. II), or devoid of an eggshell. Thus, neither a change in the overall length scale of embryos nor a removal of mechanical constraints imposed by the rigid eggshell was found to alter the relaxation behavior of the nuclei.

To probe a continuing relaxation growth of nuclei for prolonged cell cycles also with light-sheet imaging, we took advantage of our previously reported data showing a temperature dependence of cell division times in the early embryo without treatment [33]. Specifically, the time between cell divisions was observed to follow the Arrhenius law, resulting in a prolonged cell cycle when embryos were cooled from 22.5 °C to 15 °C. When analyzing nuclear volumes in these data, we did not observe a consistent variation of the temporal evolution of nuclear volumes; i.e., neither the plateau values V_S nor the relaxation timescale τ changed in a consistent manner with temperature (Fig. S2 in the Supplemental Material [48]). However, because of the longer cell cycle time at the lower temperature, the relaxation process converged closer to saturation (Fig. 3). Thus, both quantification approaches clearly show that nuclear volumes follow a relaxation process towards an asymptotic value that may not be reached for large cells due to an early onset of the next cell division.

The fit parameters extracted from Eq. (1) for all cells and available embryos (from all treatments), revealed that the minimum nuclear volume V_0 was, on average, independent of cell size [Fig. 4(a)], whereas the asymptotic volume scaled approximately linearly with cell volume, $V_S = V_0 + V_1 = \phi V_C$ with $\phi \approx 0.1$ [cf. Fig. 4(b)], in good agreement with previous observations, e.g., in fission yeast [13]. In contrast, the largest observable nuclear volume $V_N^{\max}$ showed, again, a sublinear scaling (Supplemental Material, Fig. S3). In addition, we also observed that the relaxation time τ showed a clear correlation with cell volume [Fig. 4(c)]. This correlation has not been reported before, and it clearly highlights the higher complexity and dynamic nature of the process, e.g., when trying to identify allometric relations between nuclear and cell volumes.

Based on these findings, a heuristic interpretation of the parameters in Eq. (1) seems appropriate. The minimum nuclear volume V_0 can be identified with the most compact state of the enclosed chromatin since the DNA condenses into compact chromosomes at prophase and only decondenses after anaphase, beyond which the nucleus shows a growth in volume [cf. also image sequence in Fig. 2(a)]. The asymptotic value V_S can be interpreted as the steady-state volume at which all forces that drive the initial expansion of nuclei are counterbalanced. Near or at this volume, chromatin will have reached a sufficiently decondensed state that allows not only for DNA replication but also for transcription. Finally, τ denotes the timescale required to drive nuclear expansion via the decondensing chromatin, against competing processes that aim to keep the nucleus smaller. In the next section, we will examine these events in more detail, with the goal of developing a more detailed description that can explain our experimental data and related findings.

B. Generic model for the dynamic allometry of nuclei

Before diving into the details, we provide a brief rationale for how we have constructed the model possibilities discussed in this section. Needless to say, our goal was

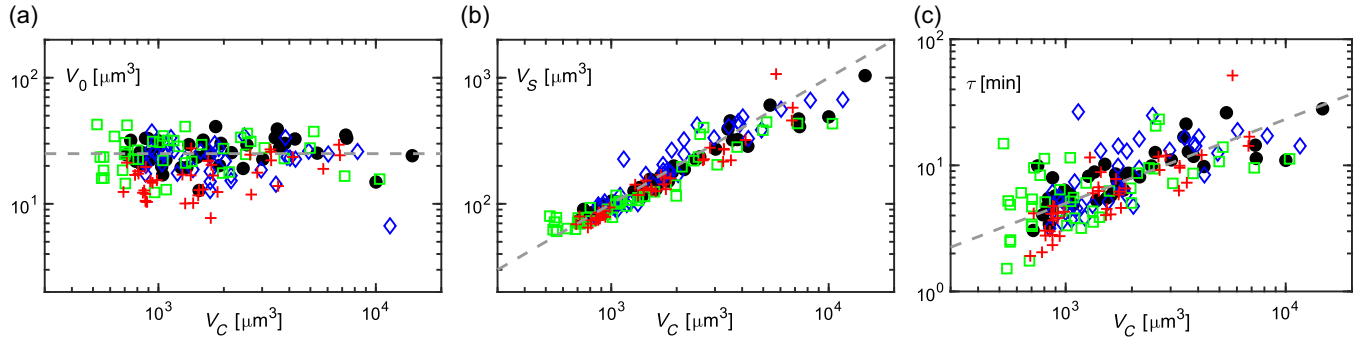

FIG. 4. (a) Starting volumes of nuclei, V_0, are, on average, constant for all cells (cf. gray dashed line); i.e., no dependency on cell volume V_C is seen. (b) The asymptotic steady-state volume of nuclei, $V_S = V_0 + V_1$, is in agreement with an isometric scaling $V_S = V_C/10$ (gray dashed line, $R^2 = 0.88$). Deviations at $V_C \approx 10^4$ μm^3 are most likely a consequence of an early interruption of the nuclear growth in cells AB and P1 [cf. Figs. 2(b) and 2(c)], which truncates the time course $V_N(t)$ and leads to an increased uncertainty of the fit parameter V_1 in Eq. (1). (c) The typical relaxation time of nuclear growth, τ, correlates with cell volume, following approximately a scaling $\tau = 0.05V_C^{2/3}$ (gray dashed line, $R^2 = 0.51$). Note that the data for untreated embryos (black circles), eggshell-devoid embryos (red crosses), smaller embryos (green squares), and larger embryos (blue diamonds) follow the same trend in all plots; i.e., neither mechanical constraints from the eggshell nor the total length of the embryo have a distinct impact. For each condition, all available cell lineages are included here.

to find a reasonable scientific explanation for our experimental data, consistent with the principle of Occam's razor. Thus, we are foremost interested in clarifying the mechanisms that determine the observed relaxation process and the resulting scaling behavior of V_S and τ. In addition, any such model needs to be consistent with earlier findings on allometric relations of nuclear and cell volumes.

Since many facets of the multiscale dynamics of chromatin and many proteins involved in nuclear size control are still unknown, our model considerations can hardly be linked to specific proteins and signaling networks, nor can we include details of the polymer physics of the highly charged chromatin strands. In essence, we have aimed for an explanation at mesoscopic scales to reveal robust physico-chemical mechanisms that cells can utilize to measure and relate two internal length scales. Although our considerations are based on and primarily targeted at the blastomeric development of *C. elegans*, possible extensions to cells growing between successive divisions are discussed at the end of this section.

1. General considerations

As a first step, we note that a relaxation law of the form depicted in Eq. (1) emerges from a differential equation of the form $dQ/dt = kQ_0 - \gamma Q$. Starting from an initial state $Q(t=0) < Q_0 k/\gamma$, $Q(t)$ follows an exponential relaxation to a steady state with a time course that is formally equivalent to Eq. (1) [after translation to volumes via $V(t) \sim Q(t)$]. Thus, two variants for the relaxation can be considered:

(i) A single process whose growth is limited by the successive depletion of a predefined and finite resource Q_0, i.e., $k = \gamma$.

(ii) A competition between two opposing processes, e.g., a constant production term kQ_0 that is opposed by a degradation term γQ with $k \neq \gamma$. This scenario features a dynamic equilibrium without a fixed finite resource that is predefined in advance.

Irrespective of these two scenarios, one has to consider an amount of chromatin that does not vary with cell size but is replicated prior to the onset of cell division. In this context, it is worthwhile to recapitulate some milestones during the cell cycle: Just before cell division, i.e., in prophase, chromatin condenses into compact chromosomes consisting of two genetically identical sister chromatids. During anaphase, sister chromatids are separated, eventually resulting in one copy per daughter cell. At the end of anaphase, a new nuclear envelope forms around the chromatids, and chromatin decondenses [see also Fig. 2(a)]. This unfolding process can be expected to exert an entropic pressure onto the nuclear envelope; i.e., it is likely to drive the observed nuclear expansion. Yet, if nuclear size were only dictated by the radius of gyration of decondensed chromatin, all cells should have nuclei of the same size. Therefore, unfolding must be limited by tuning the gyration radius of chromatin, or the cell needs to provide a force that counteracts the expansion of the polymer. Before considering reasonable mechanisms along these lines, we provide a rough quantitative estimate of the gyration radius of free chromatin and the pressure it can exert during decondensation.

For simplicity, we approximate the chromatin in *C. elegans* embryos as a single DNA polymer with an average persistence length $\ell_p \approx 50$ nm and a contour length of 0.33 nm per base pair (cf. Table 1.1 in Ref. [49]). The (haploid) genome of *C. elegans* consists of about 97×10^6 bp, which translates to a total contour length of $L \approx 64$ mm in diploid cells (assuming no compaction by histones and/or charges). The radius of gyration is therefore $R_g \approx \sqrt{L\ell_p/3} \approx 32$ μm, and doubling the

DNA during the cell cycle will even enhance this; i.e., we assume $R_g \approx 45$ μm as an upper bound for the typical extension of free chromatin. Since embryonic nuclei have radii in the range $R \approx 5$ μm, this estimate yields a typical confinement ratio $\xi = R_g/R \approx 9$.

The free energy of a polymer confined to a sphere is given by $\mathcal{F} = \alpha k_B T \xi^\beta$, with $\beta = 3/(3\nu - 1)$ [50], which yields $\beta = 15/4$ when using the Flory exponent $\nu = 3/5$. The prefactor can be estimated as $\alpha \approx 4.46$ ($R_g \approx 2R$ yields $\mathcal{F} \approx 60\, k_B T$, cf. Fig. 4 in Ref. [50]). Investing the free energy into mechanical work (expanding the nucleus) yields the maximum pressure exerted by the chromatin, $p = \mathcal{F}/V \approx 0.14$ Pa for $\xi \approx 9$. Thus, the decondensing chromatin exerts a pressure of about 140 mPa, maybe even up to 1 Pa if we consider smaller nuclei. To rate whether this is a very high pressure, we recall that (rather fragile) giant liposomes can withstand pressures of 0.1 atm $= 10^4$ Pa without deforming or bursting [51]. This comparison suggests that the nuclear envelope can easily withstand the pressure generated by chromatin without bursting. In other words, the cell does not necessarily need to compensate the expansion pressure in a fine-tuned fashion for all possible cell sizes and confinement ratios ξ. Instead, it can simply stop the expansion by imposing an invariant boundary condition, e.g., by fixing the available membrane area that can be used to build the confining nuclear envelope.

Based on these considerations, nuclear size may be tuned by two generic approaches: either by (reversibly) cross-linking the chromatin at N_c positions, which leads to a smaller gyration radius by reducing the effective contour length $L \to L/N_c$ [52], or by adjustment or restriction of the membrane area that constitutes the confining nuclear envelope. In the Supplemental Material [48], we show and discuss, in some detail, that tuning the chromatin gyration radius is, in principle, a reasonable means to set the size of the nucleus. Yet, when formulating detailed model variants, we observe either inconsistencies with experimental findings or potential instabilities; i.e., it appears implausible that cells regulate nuclear volume (only) via the gyration radius of chromatin. Therefore, in the next subsection, we will focus on developing a model based on the alternative mechanism (membrane area restriction), which yields a considerably more plausible model. Here, we repeatedly use the scaling $A \sim V^{2/3}$ since, in virtually all cases, cells and nuclei in the embryo are convex, nearly spherical objects whose volumes and surface areas are determined by the radius as $V \sim R^3$ and $A \sim R^2$.

2. Sizing nuclei by limiting the area of the nuclear envelope

As a first step in formulating the model, we note that volume-conserving cell division events cannot simultaneously conserve the membrane area. The easiest way to see this is to assume that the mother cell and the two (equally sized) daughter cells are spheres. In this case, cell division yields $V \to 2 \times V/2$ for the volume and $A = aV^{2/3} \to 2 \times a(V/2)^{2/3} \approx 1.26A$ for the area of the plasma membrane. Therefore, the total area of the plasma membrane must increase by about 25% after cell division. Even with the transient use of excess area in the fluctuating plasma membrane of the mother cell, daughter cells must either continue to live with a substantial membrane tension (which increases with each subsequent cell division) or take up membrane material from endomembranes to meet the increasing demand for a plasma membrane. In fact, it has been shown that at least the final steps of cytokinesis are fueled by vesicles from the endomembrane system that fuse with the plasma membrane [53]. Here, the term endomembrane system encompasses all organellar entities along the exocytic and endocytic pathways, such as the endoplasmic reticulum (ER), the Golgi apparatus, and endosomes. In fact, the total mass of the endomembrane system is dominated by the ER and the associated nuclear envelope, with only minor contributions from other organelles [54]. We therefore neglect these minor contributions in the following discussion.

If the endomembrane pool is not replenished, i.e., if the total membrane area is a limited resource that is set in the one-cell stage, successively smaller portions of the endomembrane system would be consumed by the plasma membrane at each division. Using spherical cells that divide into two daughter cells of equal size, it is straightforward to show that the remaining endomembrane area decreases at least proportionally with the decreasing cell volume (more likely even in a steeper, nonalgebraic way). This finding suggests that the area of the (spherical) nuclear envelope should scale at least proportionally with cell volume and the enclosed nuclear volume should at least scale as $V_C^{4/3}$, in contradiction to our experimental observation. Moreover, the assumption of a fixed amount of membrane area assumes the synthesis of phospholipids to be on hold during embryogenesis, which appears implausible.

Based on these considerations, a dynamic equilibrium of lipid synthesis, transport, and degradation—leading to relaxation scenario (ii) of the crucial membrane resource—appears more appropriate. In particular, the plasma membrane and the endomembrane system (basically, the combination of the nuclear envelope and the ER, see above) will be in dynamic equilibrium; i.e., the synthesis of new lipids (almost exclusively in the ER [55]) is counteracted by an ubiquitous degradation (e.g., by lipases). In addition, there is membrane exchange between these two pools, e.g., by vesicle- or protein-supported trafficking, or by direct contact sites [55]. We can therefore write down simple kinetic equations for the respective membrane areas:

$$\frac{dA_{\mathrm{endo}}}{dt} = k_{\mathrm{synth}} - \gamma A_{\mathrm{endo}} + \omega_i A_{\mathrm{PM}} - \omega_e A_{\mathrm{endo}}, \qquad (2)$$

$$\frac{dA_{\mathrm{PM}}}{dt} = -\gamma A_{\mathrm{PM}} - \omega_i A_{\mathrm{PM}} + \omega_e A_{\mathrm{endo}}. \tag{3}$$

Note that γ, ω_{in}, and ω_{ex} are, by definition, simple rates for area loss and exchange, whereas the area production rate due to lipid synthesis, k_{synth}, has units of an area per time. At steady state, i.e., sufficiently long after cell division, the time derivatives in Eqs. (2) and (3) vanish, yielding (after isolating A_{PM} on the left in both equations)

$$A_{\mathrm{PM}} = \frac{\gamma + \omega_e}{\omega_i} A_{\mathrm{endo}} - \frac{k_{\mathrm{synth}}}{\omega_i}, \tag{4}$$

$$A_{\mathrm{PM}} = \frac{\omega_e}{\gamma + \omega_i} A_{\mathrm{endo}}. \tag{5}$$

Approximating cells and nuclei as spherical objects, the area of the plasma membrane will have to scale at steady state with cell volume as $A_{\mathrm{PM}} \sim V_C^{2/3}$. As a consequence, Eq. (5) yields the same scaling for the endomembrane area, $A_{\mathrm{endo}} \sim A_{\mathrm{PM}} \sim V_C^{2/3}$. The endomembrane pool is essentially the union of ER tubules and the nuclear envelope (see above), i.e., $A_{\mathrm{endo}} = A_N + A_{\mathrm{ER}}$. Furthermore, in most eukaryotes, including *C. elegans*, the ER and the nuclear envelope form an interconnected membrane system along which membrane material (lipids) can be exchanged by simple diffusion [56,57]. Therefore, the dynamic balance of the nuclear envelope area can be described by a simple rate equation, $dA_N/dt = \kappa_{\mathrm{in}} A_{\mathrm{ER}} - \kappa_{\mathrm{out}} A_N$, yielding $A_N \sim A_{\mathrm{ER}} \sim A_{\mathrm{endo}} \sim V_C^{2/3}$ at steady state. Combined with the relation $A_N \sim V_N^{2/3}$, this yields the experimentally observed isometry $V_N \sim V_C$ at steady state.

A key component in the above derivation is lipid homeostasis, as this ensures the balance between the endomembrane pool and the plasma membrane [Eqs. (2) and (3)]. Therefore, a prediction of the model is that an increased rate of lipid synthesis should result in larger steady-state volumes of nuclei. In agreement with this prediction, deletion of *cnep-1*, a negative regulator of ER membrane biogenesis, increased the endomembrane pool in early *C. elegans* embryos and resulted in significantly larger nuclei [58]. Our line of reasoning is further supported by data from sea-urchin embryos in which ER membranes were found to be important drivers of nuclear growth [26], and by data from fission yeast, indicating that the ER and its associated lipid synthesis are regulators of nuclear size [59].

Beyond steady-state considerations, we also need to explain the correlation of nuclear relaxation times with cell volume [Fig. 4(c)]. To this end, we recall that ER membranes form a vast network that is interconnected with the nuclear envelope in virtually all cells [56] [cf. sketch in Fig. 5(a)]. This extended network is established and maintained by several mechanisms, including interactions of ER tubules

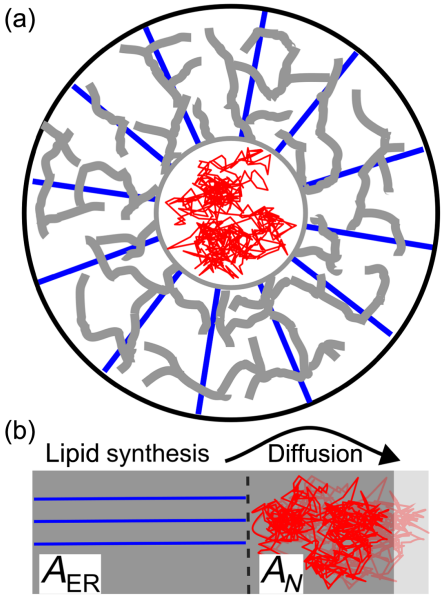

FIG. 5. (a) Two-dimensional sketch of an idealized, spherical cell. The expanding chromatin (red) aims at increasing the nuclear envelope (gray circle in the center) whereas the connected and contiguous ER membrane tubules (gray lines) are spread along radially arranged microtubules (blue rods). Multiple interactions with the cytoskeleton and contact sites with the plasma membrane expand the vast ER network, hence limiting the available membrane pool for nuclear growth; see main text for details. (b) Fixing the ER membrane area in the vast network limits the available material for the nuclear envelope. The nucleus has to withstand the pressure from decondensed chromatin until nascent lipids (synthesized in the ER) diffuse to the nuclear envelope and get trapped there, hence relaxing the pressure by a surface area increase; see main text for details.

with the stiff microtubule cytoskeleton, with the actomyosin cortex beneath the plasma membrane, and through specialized protein complexes (so-called contact sites) with the plasma membrane [56]. Moreover, the ER network remains partially extended even during cell division, and it rapidly reextends throughout the cell again after mitosis, in mammalian culture cells [60] and in *C. elegans* embryos [61], hence fixing the ER fraction of the endomembrane pool. Indeed, disruption of the actin cytoskeleton in *C. elegans* embryos was seen to impair the dispersal of ER structures throughout the cell at the end of mitosis [61]. Assuming that these manifold interactions (that expand the ER) always outcompete the chromatin-derived forces (that attempt to increase the nuclear envelope area at the expense of the ER), chromatin expansion cannot simply redistribute the membrane area from the ER to the nuclear membrane. Consequently, the nuclear growth can only be fed by newly added membrane material. Having supplemented the plasma membrane during cytokinesis, the endomembrane system suffers from a lack of lipids after cell division, which is compensated by the synthesis of new lipids in the ER [cf. Eq. (2)]. Diffusion of these nascent lipids within the

interconnected endomembrane system will eventually contribute additional material to the nuclear envelope [cf. sketch in Fig. 5(b)]. As these newly arrived lipids allow for nuclear expansion, the free energy of the enclosed chromatin will decrease, and the diffusion of lipids out of the nuclear envelope becomes unfavorable. Thus, lipids are trapped in the nuclear envelope, similar to a diffuse-to-capture scenario. This result allows the nucleus to expand until Eq. (2) approaches a steady state. Since nascent lipids diffusively explore the ER until they get trapped in the nuclear envelope, the relaxation time can be estimated from the mean square displacement as $\tau \sim A_{\mathrm{ER}}/D \sim V_C^{2/3}$. This prediction of the scaling of τ is in favorable agreement with our experimental data [cf. Fig. 4(c)], even though the scatter in the data prevents a too-close comparison.

For a more quantitative estimate, we consider a typical diffusion constant $D \approx 1\ \mu\mathrm{m}^2/\mathrm{s}$ of lipids in membranes and a typical cell volume $V_C \approx 4000\ \mu\mathrm{m}^3$ in the embryo. EM studies have revealed an area of 10 $\mu\mathrm{m}^2$ of ER membrane per $\mu\mathrm{m}^3$ of cytoplasm (Table 1 in Ref. [62]), yielding an estimate of $40,000\ \mu\mathrm{m}^2$ of ER membrane area in embryonic cells. Since lipid production sites are distributed throughout the ER, nascent lipids must travel different distances to reach the nuclear envelope. On average, lipids may have to explore only about 10% of the ER before reaching the nuclear envelope, suggesting a search time of $\tau = 4000\ \mu\mathrm{m}^2/(4D) \approx 15$ min. This very rough estimate is consistent with the observed magnitude of timescales for nuclear growth, providing additional support for our line of argumentation.

Therefore, a reasonable model for our experimental data is as follows: Homeostasis of cellular membranes results in a dynamically maintained steady-state area of endomembranes with a scaling $A_N \sim A_{\mathrm{ER}} \sim A_{\mathrm{endo}} \sim V_C^{2/3}$. This yields a steady-state volume of nuclei that scales linearly with cell volume, $V_N \sim A_N^{3/2} \sim V_C$, in agreement with our experimental data [Fig. 4(b)] and previous observations in mouse macrophages [18], mammalian culture cells [22], and fission yeast [13]. After mitosis, the endomembrane area is below steady-state levels, but the ER is rapidly expanded to and/or maintained at its maximal size. Lipid synthesis replenishes the endomembrane pool, and nascent lipids will undergo a diffusion-limited trapping scenario, providing new membrane material in the nuclear envelope. Then, the nucleus can grow with a relaxation time that scales as $\tau \sim A_{\mathrm{ER}} \sim V_C^{2/3}$, in line with our data [Fig. 4(c)].

DNA replication between successive cell divisions increases the pressure on the nuclear envelope, but the ER remains extended, limiting the available membrane for nuclear expansion. As a result, the nucleus cannot grow further but needs to withstand the higher pressure, in agreement with a lack of expansion during DNA replication. Reducing the amount of DNA in each cell should also have little to no effect, in accordance with the observation of an unaltered nuclear size in haploid *C. elegans* embryos [63]. Another interesting feature of this model is the almost constant value of diffusion constants $D \propto k_B T$ in the embryo's physiological range (15–25 °C yields barely a 3% change in absolute temperature), suggesting constant relaxation times of nuclei. This result is consistent with our observations (Figs. 3 and S2 in the Supplemental Material [48]).

Since this model of nuclear envelope area restriction invokes a general lipid homeostasis but does not depend directly on the amount of DNA, nor on the production of proteins or their import into nuclei, it also provides an explanation for the observations of isometric nuclear size in growing yeast cells under several perturbations [64], including a blocked protein synthesis. Similarly, the model is also expected to hold for mammalian cells, irrespective of ploidy: The slow cell growth (on the timescale of hours) seen for mammalian embryos or culture cells is much slower than the relaxation of nuclei; i.e., the nucleus has enough time to relax before the next cell division. A slow increase in cell volume, plasma membrane, and endomembrane areas hence occurs in a quasi-steady state in which the isometric scaling $V_N \sim V_C$ is maintained (all components essentially grow with the same slow rate). Only when the balance of forces between the ER membrane and the nuclear envelope is massively perturbed, e.g., due to a massive dysregulation of protein expression levels, can one expect marked deviations from the model predictions, which may explain why highly dysregulated cancer cells can deviate from an isometric scaling.

Finally, it is also worth noting that mammalian cells feature considerably longer chromatin contour lengths, up to $L \approx 1$ m. Therefore, it can be expected that additional mechanisms, such as the discussed cross-linking of chromatin [48], may further supplement the basic mechanism of limiting the available membrane for the nuclear envelope.

IV. CONCLUSION

In conclusion, we have shown here that nuclei in *C. elegans* embryos undergo relaxation growth, which results in a dynamic allometry of nuclear and cell volume, $V_N \sim V_C^{\alpha}$; i.e., the scaling exponent α depends on the time at which the nucleus volume is quantified. Since cell division times are inversely correlated with cell volume in the early embryo [32], large cells interrupt the relaxation growth of nuclei due to an early onset of mitosis. Monitoring nuclear volume just before mitosis therefore yields a sublinear allometry, whereas the asymptotic nuclear volume (after a full relaxation) follows an isometric scaling $V_N \sim V_C$. Moreover, the relaxation time of nuclei is seen to roughly follow a scaling $\tau \sim V_C^{2/3}$. All of these findings are explained by a model in which the available membrane for the nuclear envelope is limited by the extended ER network. This model is also consistent with previous findings on nuclear size in yeast under varying conditions [13,64]. The model provides a robust

physico-chemical explanation for the (dynamically) maintained isometry of nucleus and cell volume, preventing overly large nuclei that possibly restrain and hamper vital processes in the cytoplasm. Certainly, advanced biochemical pathways with cell- and species-specific regulatory mechanisms might be added, equipping the basic mechanism with additional redundance and robustness.

ACKNOWLEDGMENTS

Some strains were provided by the Caenorhabditis Genetics Center funded by the NIH Office of Research Infrastructure Programs (P40 OD010440). R. F. and M. W. gratefully acknowledge financial support by the DFG (Grant No. WE4335/3-2), by BayFor (BayIntAn, UBT2017-26), and by the VolkswagenStiftung (Az. 92738). This article is funded by the Open Access Publishing Fund of the University of Bayreuth. A. K. thanks Jonathon Howard (Yale University) for discussion on nuclear size scaling, and gratefully acknowledges financial support by JSPS KAKENHI (Grants No. JP18H02414, No. JP18H05529, and No. JP18KK0202).

[1] R. H. Peters, *The Ecological Implications of Body Size*, Cambridge Studies in Ecology (Cambridge University Press, Cambridge, England, 1983).
[2] A. F. Wright, S. G. Jacobson, A. V. Cideciyan, A. J. Roman, X. Shu, D. Vlachantoni, R. R. McInnes, and R. A. Riemersma, *Lifespan and mitochondrial control of neurodegeneration*, Nat. Genet. **36**, 1153 (2004).
[3] S. Uppaluri, S. C. Weber, and C. P. Brangwynne, *Hierarchical size scaling during multicellular growth and development*, Cell Rep. **17**, 345 (2016).
[4] *The Evolution of the Genome*, edited by T. R. Gregory (Academic Press, New York, 2005).
[5] K. P. Baetcke, A. H. Sparrow, C. H. Nauman, and S. S. Schwemmer, *The relationship of DNA content to nuclear and chromosome volumes and to radiosensitivity (LD50)*, Proc. Natl. Acad. Sci. U.S.A. **58**, 533 (1967).
[6] C. C. Henery and M. H. Kaufman, *Relationship between cell size and nuclear volume in nucleated red blood cells of developmentally matched diploid and tetraploid mouse embryos*, J. Exp. Zool. **261**, 472 (1992).
[7] G. Fankhauser, *The effects of changes in chromosome number on amphibian development*, Q. Rev. Biol. **20**, 20 (1945).
[8] R. Hertwig, *Über Korrelation von Zell-und Kerngröße und ihre Bedeutung für die geschlechtliche Differenzeierung und die Teilung der Zelle*, Biol. Centralblatt. **23**, 49 (1903).
[9] T. Boveri, *Über die Abhängigkeit der Kerngröße und Zellenzahl der Seeigel-Larven von der Chromosomenzahl der Ausgangszellen* (Zellen-Studien (Heft 5), Verlag Gustav Fischer, Jena, 1905).
[10] Edwin G. Conklin, *Cell size and nuclear size*, J. Exp. Zool. **12**, 1 (1912).
[11] E. B. Wilson, *The cell in development and heredity* (MacMillan, New York, 1925).
[12] P. Jorgensen, N. P. Edgington, B. L. Schneider, I. Rupes, M. Tyers, and B. Futcher, *The size of the nucleus increases as yeast cells grow*, Mol. Biol. Cell. **18**, 3523 (2007).
[13] F. R. Neumann and P. Nurse, *Nuclear size control in fission yeast*, J. Cell Biol. **179**, 593 (2007).
[14] Y. Hara and A. Kimura, *Cell-size-dependent spindle elongation in the Caenorhabditis elegans early embryo*, Curr. Biol. **19**, 1549 (2009).
[15] D. L. Levy and R. Heald, *Nuclear size is regulated by importin α and NTF2 in Xenopus*, Cell **143**, 288 (2010).
[16] L. J. Edens, K. H. White, P. Jevtic, X. Li, and D. L. Levy, *Nuclear size regulation: From single cells to development and disease*, Trends Cell Biol. **23**, 151 (2013).
[17] H. Cantwell and P. Nurse, *Unravelling nuclear size control*, Curr. Genet. **65**, 1281 (2019).
[18] J. A. Swanson, M. Lee, and P. E. Knapp, *Cellular dimensions affecting the nucleocytoplasmic volume ratio*, J. Cell Biol. **115**, 941 (1991).
[19] F. Han, P. Liang, F. Wang, L. Zeng, and B. Zhang, *Automated analysis of time-lapse imaging of nuclear translocation by retrospective strategy and its application to STAT1 in HeLa cells*, PLoS One **6**, e27454 (2011).
[20] D. Zink, A. H. Fischer, and J. A. Nickerson, *Nuclear structure in cancer cells*, Nat. Rev. Cancer **4**, 677 (2004).
[21] P. Jevtic and D. L. Levy, *Mechanisms of nuclear size regulation in model systems and cancer*, Adv. Exp. Med. Biol. **773**, 537 (2014).
[22] Y. Wu, A. F. Pegoraro, D. A. Weitz, P. Janmey, and S. X. Sun, *The correlation between cell and nucleus size is explained by an eukaryotic cell growth model*, PLoS Comput. Biol. **18**, e1009400 (2022).
[23] A. K. Yesbolatova, R. Arai, T. Sakaue, and A. Kimura, *Formulation of chromatin mobility as a function of nuclear size during C. elegans embryogenesis using polymer physics theories*, Phys. Rev. Lett. **128**, 178101 (2022).
[24] N. W. Goehring and A. A. Hyman, *Organelle growth control through limiting pools of cytoplasmic components*, Curr. Biol. **22**, R330 (2012).
[25] Y. Hara and C. A. Merten, *Dynein-based accumulation of membranes regulates nuclear expansion in Xenopus laevis egg extracts*, Dev. Cell. **33**, 562 (2015).
[26] R. N. Mukherjee, J. Salle, S. Dmitrieff, K. M. Nelson, J. Oakey, N. Minc, and D. L. Levy, *The perinuclear ER scales nuclear size independently of cell size in early embryos*, Dev. Cell. **54**, 395 (2020).
[27] P. Chen, M. Tomschik, K. M. Nelson, J. Oakey, J. C. Gatlin, and D. L. Levy, *Nucleoplasmin is a limiting component in the scaling of nuclear size with cytoplasmic volume*, J. Cell Biol. **218**, 4063 (2019).
[28] C. Brownlee and R. Heald, *Importin alpha partitioning to the plasma membrane regulates intracellular scaling*, Cell **176**, 805 (2019).
[29] K. Kume, H. Cantwell, F. R. Neumann, A. W. Jones, A. P. Snijders, and P. Nurse, *A systematic genomic screen implicates nucleocytoplasmic transport and membrane growth in nuclear size control*, PLoS Genet. **13**, e1006767 (2017).
[30] P. Gonczy and L. S. Rose, *Asymmetric cell division and axis formation in the embryo*, WormBook (2005), 10.1895/wormbook.1.30.1.

[31] R. Fickentscher, P. Struntz, and M. Weiss, *Mechanical cues in the early embryogenesis of Caenorhabditis elegans*, Biophys. J. **105**, 1805 (2013).
[32] R. Fickentscher, P. Struntz, and M. Weiss, *Setting the clock for fail-safe early embryogenesis*, Phys. Rev. Lett. **117**, 188101 (2016).
[33] R. Fickentscher, S. W. Krauss, and M. Weiss, *Anti-correlation of cell volumes and cell-cycle times during the embryogenesis of a simple model organism*, New J. Phys. **20**, 113001 (2018).
[34] Y. Hara and A. Kimura, *An allometric relationship between mitotic spindle width, spindle length, and ploidy in Caenorhabditis elegans embryos*, Mol. Biol. Cell **24**, 1411 (2013).
[35] Y. Hara, M. Iwabuchi, K. Ohsumi, and A. Kimura, *Intranuclear DNA density affects chromosome condensation in metazoans*, Mol. Biol. Cell. **24**, 2442 (2013).
[36] G. Greenan, C. P. Brangwynne, S. Jaensch, J. Gharakhani, F. Julicher, and A. A. Hyman, *Centrosome size sets mitotic spindle length in Caenorhabditis elegans embryos*, Curr. Biol. **20**, 353 (2010).
[37] A. Carvalho, A. Desai, and K. Oegema, *Structural memory in the contractile ring makes the duration of cytokinesis independent of cell size*, Cell **137**, 926 (2009).
[38] S. C. Weber and C. P. Brangwynne, *Inverse size scaling of the nucleolus by a concentration-dependent phase transition*, Curr. Biol. **25**, 641 (2015).
[39] A. Audhya, F. Hyndman, I. X. McLeod, A. S. Maddox, J. R. Yates, A. Desai, and K. Oegema, *A complex containing the Sm protein CAR-1 and the RNA helicase CGH-1 is required for embryonic cytokinesis in Caenorhabditis elegans*, J. Cell Biol. **171**, 267 (2005).
[40] A. Audhya, A. Desai, and K. Oegema, *A role for Rab5 in structuring the endoplasmic reticulum*, J. Cell Biol. **178**, 43 (2007).
[41] S. Brenner, *The genetics of Caenorhabditis elegans*, Genetics **77**, 71 (1974).
[42] M. Brauchle, K. Baumer, and P. Goenczy, *Differential activation of the DNA replication checkpoint contributes to asynchrony of cell division in C. elegans embryos*, Curr. Biol. **13**, 819 (2003).
[43] H. Stevens, A. B. Williams, and W. M. Michael, *Cell-type specific responses to DNA replication stress in early C. elegans embryos*, PLoS One **11**, e0164601 (2016).
[44] Karen McNally, Anjon Audhya, Karen Oegema, and Francis J. McNally, *Katanin controls mitotic and meiotic spindle length*, J. Cell Biol. **175**, 881 (2006).
[45] Philipp Struntz and Matthias Weiss, *Multiplexed measurement of protein diffusion in Caenorhabditis elegans embryos with SPIM-FCS*, J. Phys. D **49**, 044002 (2016).
[46] R. Fickentscher and M. Weiss, *Physical determinants of asymmetric cell divisions in the early development of Caenorhabditis elegans*, Sci. Rep. **7**, 9369 (2017).
[47] P. Askjaer, V. Galy, E. Hannak, and I. W. Mattaj, *Ran GTPase cycle and importins alpha and beta are essential for spindle formation and nuclear envelope assembly in living Caenorhabditis elegans embryos*, Mol. Biol. Cell. **13**, 4355 (2002).
[48] See Supplemental Material at http://link.aps.org/supplemental/10.1103/PhysRevX.14.011016 for additional experimental results and model considerations.
[49] Rob Phillips, *Physical biology of the cell*, 2nd ed. (Garland Science, Taylor and Francis Group, New York, NY, 2015).
[50] Angelo Cacciuto and Erik Luijten, *Self-avoiding flexible polymers under spherical confinement*, Nano Lett. **6**, 901 (2006).
[51] Xiaoyan Liu, Joakim Stenhammar, Håkan Wennerström, and Emma Sparr, *Vesicles balance osmotic stress with bending energy that can be released to form daughter vesicles*, J. Phys. Chem. Lett. **13**, 498 (2022).
[52] Y. Kantor and M. Kardar, *Conformations of randomly linked polymers*, Phys. Rev. E **54**, 5263 (1996).
[53] Stephane Fremont and Arnaud Echard, *Membrane traffic in the late steps of cytokinesis*, Curr. Biol. **28**, R458 (2018).
[54] D. N. Itzhak, S. Tyanova, J. Cox, and G. H. H. Borner, *Global, quantitative and dynamic mapping of protein subcellular localization*, eLife **5**, e16950 (2016).
[55] Bruce Alberts, *Molecular Biology of the Cell*, 6th ed. (Garland Science, Taylor and Francis Group, New York, NY, 2015).
[56] L. M. Westrate, J. E. Lee, W. A. Prinz, and G. K. Voeltz, *Form follows function: The importance of endoplasmic reticulum shape*, Annu. Rev. Biochem. **84**, 791 (2015).
[57] Z. Y. Lee, M. Prouteau, M. Gotta, and Y. Barral, *Compartmentalization of the endoplasmic reticulum in the early C. elegans embryos*, J. Cell Biol. **214**, 665 (2016).
[58] M. S. Mauro, G. Celma, V. Zimyanin, M. M. Magaj, K. H. Gibson, S. Redemann, and S. Bahmanyar, *Ndc1 drives nuclear pore complex assembly independent of membrane biogenesis to promote nuclear formation and growth*, eLife **11**, e75513 (2022).
[59] K. Kume, H. Cantwell, A. Burrell, and P. Nurse, *Nuclear membrane protein Lem2 regulates nuclear size through membrane flow*, Nat. Commun. **10**, 1871 (2019).
[60] M. Puhka, H. Vihinen, M. Joensuu, and E. Jokitalo, *Endoplasmic reticulum remains continuous and undergoes sheet-to-tubule transformation during cell division in mammalian cells*, J. Cell Biol. **179**, 895 (2007).
[61] D. Poteryaev, J. M. Squirrell, J. M. Campbell, J. G. White, and A. Spang, *Involvement of the actin cytoskeleton and homotypic membrane fusion in ER dynamics in Caenorhabditis elegans*, Mol. Biol. Cell **16**, 2139 (2005).
[62] D. Paumgartner, G. Losa, and E. R. Weibel, *Resolution effect on the stereological estimation of surface and volume and its interpretation in terms of fractal dimensions*, J. Microsc. **121**, 51 (1981).
[63] Hanako Hayashi, Kenji Kimura, and Akatsuki Kimura, *Localized accumulation of tubulin during semi-open mitosis in the Caenorhabditis elegans embryo*, Mol. Biol. Cell. **23**, 1688 (2012).
[64] P. Jorgensen, N. P. Edgington, B. L. Schneider, I. Rupes, M. Tyers, and B. Futcher, *The size of the nucleus increases as yeast cells grow*, Mol. Biol. Cell. **18**, 3523 (2007).